Indian Journal of Pure & Applied Physics
Vol. 56, January 2018, pp. 34-47

Spectroscopic and quantum mechanical investigations of (2*E*)-3-(2*H*-1,3-benzodioxol-5-yl)-*N*-phenylprop-2-enamide using density functional theory method

S Abbas Manthri[a], R Raj Muhamed[a], R Rajesh[a] & V Sathyanarayanamoorthi[b]*

[a]Department of Physics, Jamal Mohamed College, Tiruchirappalli 620 020, India
[b]Department of Physics, PSG College of Arts and Science, Coimbatore 641 014, India

Received 15 September 2016; accepted 31 October 2017

The Fourier transform infrared (FTIR) and FT-Raman of (2*E*)-3-(2*H*-1,3-benzodioxol-5-yl)-*N*-phenylprop-2-enamide (2BNP2E) have been recorded in the regions 4000-100 and 4000-450cm^{-1}, respectively. A complete assignment and analysis of the fundamental vibrational modes of the molecule have been carried out. The observed fundamental modes have been compared with the harmonic vibrational frequencies computed using DFT (B3LYP) method by employing 6-311++G(d,p) basis set. The vibrational studies have been interpreted in terms of potential energy distribution. The first order hyperpolarizability (β_0) and related properties (α, μ and $\Delta\alpha$) of this molecular system are calculated using B3LYP/6-311++G(d,p) method based on the finite-field approach. Stability of the molecule arising from hyperconjugative interactions and charge delocalization has been analyzed using natural bond orbital (NBO) analysis. The results show that electron density (ED) in the σ^* and π^* anti-bonding orbitals and second-order delocalization energies ($E(2)$) confirm the occurrence of intramolecular charge transfer (ICT) within the molecule. Molecular electrostatic potential (MEP) and HOMO-LUMO energy levels have also been constructed. The thermodynamic properties of the title compound have been calculated at different temperature and the results reveal that the standard heat capacity $C^0_{p,m}$, entropy S^0_m and enthalpy changes H^0_m increase with rise in temperature.

Keywords: DFT, FTIR, FT-Raman, HOMO-LUMO, MEP, NLO

1 Introduction

1,3-benzodioxole moiety occurs commonly in many antimitotic agents such as podophyllotoxin, steganacin, and combretastatin[1] A-2. In mid 80s, a number of 1,3-benzodioxoles were reported to be active in vivo against P388 lymphocytic leukaemia and other tumors and, like podophyllotoxin, to be potent tubulin binders and antimitotic agents[2,3]. Furthermore, it has been recently reported that a series of 1,3-benzodioxole derivatives possess a cytotoxic activity against several human tumor cell lines including human colon carcinoma cells[4] and multi drug-resistant nasopharyngeal carcinoma cells[5]. 1, 3-benzodioxole derivatives of these natural products are used as inhibitors of mono-oxygenase enzymes, pesticides or pesticide intermediates, herbicides, antioxidants, antimicrobials, and medicines[6]. On this basis and in pursuing our interest in the discovery of new anticancer agents[7,8], we have recently focused our attention on new 1,3-benzodioxole derivatives[9].

In the present study, it is planned to have a joint experimental and theoretical investigation of FTIR and FT-Raman spectra. Literature survey reveals that so far there is no complete theoretical study was carried out for 2BNP2E. Additionally, it was also planned to illuminate theoretical determination of the optimized molecular geometries, HOMO-LUMO energy gap, MEP, NLO, NBO and thermo dynamical analysis of the title compound by using density functional theory (DFT) with B3LYP/6-311++G(d,p) basis set. The other important quantities such as ionization potential, electron affinity, electrophilicity index, chemical potential, electronegativity, hardness, and softness are also evaluated in the way of molecular orbital framework. In the paper, all calculations are valuable for providing insight into molecular properties of title compound.

*Corresponding author
(E-mail: sathyanarayanamoorthi@yahoo.co.in)

2 Synthesis

It was prepared by dissolving equivalent weight of (1:1 mole) N-phenylacetamide and benzo[d][1,3] dioxole-5-carbaldehyde in absolute ethanol (20 mL), to form a yellow colour liquid. The sodium hydroxide (40% in 1 ml) in water was added drop wise to the mixture to form a yellow colour liquid. Then, the mixture was refluxed for 3 h at 40 °C. The reaction was monitored by TLC, after the completion of reaction; it was dried and washed with pet ether solvent. The separated solid was recrystallized with ethanol.

3 Experimental

The FTIR spectrum of the synthesis compound (2*E*)-3-(2*H*-1,3-benzodioxol-5-yl)-*N*-phenylprop-2-enamide (2BNP2E) was recorded in the region 4000-450 cm^{-1} in evacuation mode using a KBr pellet technique with 1.0 cm^{-1} resolution on a PERKIN ELMER FTIR spectrophotometer. The FT-Raman spectrum of the 2BNP2E compound was recorded in the region 4000-100 cm^{-1} in a pure mode using Nd: YAG Laser of 100 mW with 2 cm^{-1} resolution on a BRUCKER RFS 27 at SAIF, IIT Chennai, India.

4 Computational Details

The entire calculations were performed at DFT (B3LYP) levels on a personal computer using[10] Gaussian 03W program package, invoking gradient geometry optimization[11]. The harmonic vibrational frequencies were calculated at the same level of theory for the optimized structures and obtained frequencies were scaled[12] by 0.961. The spectra were analyzed in terms of the PED aid by using the VEDA program[13]. The natural bonding orbital (NBO) calculation was performed using NBO 3.1 program[14] and was implemented in the Gaussian 03W package at the B3LYP/ 6-311++G(d,p) basis set.

5 Results and Discussion

5.1 Molecular geometry

The numbering system adopted in the molecular structure of 2BNP2E is shown in Fig. 1. The optimized structure parameters of this compound calculated DFT/B3LYP levels with the 6-311++G(d,p) basis set are listed in Table 1. Since the crystal structure of this 2BNP2E is not available in the literature. Therefore, the crystal data of a closely related molecule such as (E)-2-Cyano-3-[4-(dimethylamino)-phenyl]-N-phenylprop-2-enamide[15] is compared with that of the title compound. It is observed that the calculated C-C bond distances are higher than the other bond lengths such as C-O, C-N, C-H, N-H and O-C they are found to be slight difference at all levels of calculations. The calculated of C-H bond length is slightly higher than the observed C-H bond length is 1.089 Å. The C-N, C-O and O-C bond distances calculated by B3LYP/6-311++G(d,P) methods are higher than the observed result. Most of the bond lengths and bond angles are slightly deviate when comparing with the experimental data[15] for both DFT functional. These differences are probably due to the theoretical calculations belong to isolated molecule in gaseous phase while the experimental results belongs to molecule in solid state. All calculated geometrical parameters obtained at the DFT level of theory are in good agreement with the experimental structural parameters. Despite these differences, the calculated geometrical parameters represent a good approximation, and they are the basis for the calculation of other parameters such as polarizability, vibrational frequencies and thermodynamical properties which are described in the following sessions.

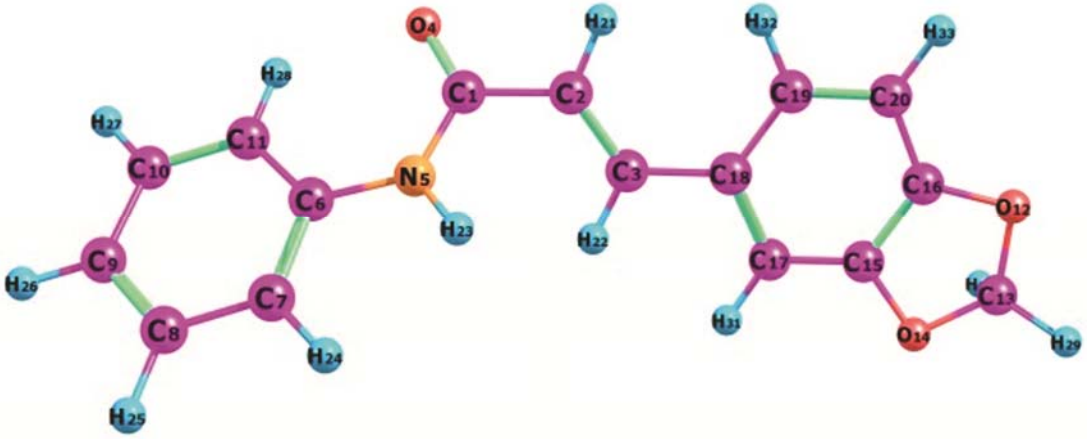

Fig. 1 — The theoretical optimized geometric structure with atoms numbering of 2BNP2E.

Table 1 — Optimized geometrical parameters of (2E)-3-(2H-1,3-benzodioxol-5-yl)-N-phenylprop-2-enamide obtain by B3LYP/6-311++G(d,p) basis set (*Contd.*).

Parameters	Experimental[a]	B3LYP/ 6-311++G(d,p)	% error	Parameters	Experimental[a]	B3LYP/ 6-311++G(d,p)	% error
Bond length (Å)							
C1-C2	1.493	1.487	0.402	C18-C3-H22	114	113.9	0.088
C1-O4	1.216	1.223	-0.576	C3-C18-C17	118.2	117.9	0.254
C1-N5	1.359	1.38	-1.545	C3-C18-C19	122.4	122.8	-0.327
C2-C3	1.358	1.343	1.105	C6-N5-H23	116	114.8	1.034
C2-H21	0.96	1.084	-12.917	N5-C6-C7	116.3	117.1	-0.688
C3-C18	1.442	1.466	-1.664	N5-C6-C11	124.7	123.6	0.882
C3-H22	0.96	1.089	-13.438	C7-C6-C11	119.4	119.3	0.084
N5-C6	1.385	1.41	-1.805	C6-C7-C8	120.6	120.6	0.000
N5-H23	0.96	1.008	-5.000	C6-C7-H24	119	119.6	-0.504
C6-C7	1.385	1.403	-1.300	C6-C11-C10	119.4	119.4	0.000
C6-C11	1.385	1.401	-1.155	C6-C11-H28	120	119.6	0.333
C7-C8	1.385	1.389	-0.289	C8-C7-H24	120	119.7	0.250
C7-H24	0.96	1.086	-13.125	C7-C8-C9	119.9	120.2	-0.250
C8-C9	1.385	1.395	-0.722	C7-C8-H25	119	119.4	-0.336
C8-H25	0.96	1.084	-12.917	C9-C8-H25	120	120.3	-0.250
C9-C10	1.397	1.393	0.286	C8-C9-C10	119	119.1	-0.084
C9-H26	0.96	1.084	-12.917	C8-C9-H26	120	120.4	-0.333
C10-C11	1.397	1.394	0.215	C10-C9-H26	120	120.5	-0.417
C10-H27	0.96	1.084	-12.917	C9-C10-C11	121.3	121.4	-0.082
C11-H28	0.96	1.079	-12.396	C9-C10-H27	120	119.9	0.083
C12-C13	1.424	1.436	-0.843	C11-C10-H27	119	118.7	0.252
C12-C16	1.363	1.37	-0.514	C10-C11-H28	120	121	-0.833
C13-O14	1.424	1.433	-0.632	C13-C12-C16	116.1	105.2	9.388
C13-H29	0.96	1.089	-13.438	C12-C13-C14	121.2	107.2	11.551
C13-H30	0.96	1.097	-14.271	C12-C13-H29	114	109.4	4.035
O14-C15	1.216	1.374	-12.993	C12-C13-H13	114	109.2	4.211
C15-C16	1.39	1.39	0.000	C12-C16-C15	116.8	109.7	6.079
C15-C17	1.375	1.375	0.000	C12-C16-C20	125.7	128.7	-2.387
C16-C20	1.379	1.381	-0.145	C14-C13-H29	114	109.5	3.947
C17-C18	1.407	1.416	-0.640	C14-C13-H30	114	109.4	4.035
C17-H31	0.96	1.083	-12.813	C13-C14-C15	116.1	105.2	9.388
C18-C19	1.407	1.404	0.213	H29-C13-H30	110	111.9	-1.727
C19-C20	1.397	1.399	-0.143	C14-C15-C16	116.1	109.5	5.685
C19-H32	0.96	1.082	-12.708	C14-C15-C17	125.7	128.5	-2.228
C20-H33	0.96	1.082	-12.708	C16-C15-C17	121.9	122	-0.082
C2-C1-O4	121.2	120.4	0.660	C15-C17-C18	118.2	117.9	0.254
C2- C1-N5	116.3	115.8	0.430	C15-C17-H31	120	120.9	-0.750
C1-C2-C3	125.7	126.2	-0.398	C16-C20-C19	117.7	117.1	0.510
C1-C2-H21	114	112.1	1.667	C16-C20-H33	120	121.3	-1.083

(*Contd.*)

Table 1 — Optimized geometrical parameters of (2E)-3-(2H-1,3-benzodioxol-5-yl)-N-phenylprop-2-enamide obtain by B3LYP/6-311++G(d,p) basis set.

Parameters	Experimental[a]	B3LYP/ 6-311++G(d,p)	% error	Parameters	Experimental[a]	B3LYP/ 6-311++G(d,p)	% error
Bond length (Å)							
O4-C1-N5	124	123.8	0.161	C18-C17-H31	120	121.2	-1.000
C1-N5-C6	128.4	129.3	-0.701	C17-C18-C19	119.9	119.3	0.500
C1-N5-H23	116	115.7	0.259	C18-C19-C20	121.09	122.1	-0.834
C3-C2-H21	120	121.5	-1.250	C18-C19-H32	119	119.6	-0.504
C2-C3-C18	125.7	127.6	-1.512	C20-C19-H32	119	118.3	0.588
C2-C3-H22	119	118.5	0.420	C19-C20-H33	120	121.6	-1.333

[a] Ref.[15]

5.2 Vibrational analysis

The 2BNP2E molecule has C1 point group symmetry and 33 atoms, hence it has 93 (i.e., 3n-6) normal vibrational modes, which are found to be active in both IR and Raman scattering simultaneously are collected in Table 2. Theoretical wavenumbers of vibrations, Raman activity and IR intensity have been computed at the DFT/B3LYP/6-311++G(d,p) level. The quantum chemical methods overestimate the force constants at the exact equilibrium geometry which results in higher value of calculated harmonic wavenumbers than the corresponding experimental ones. These discrepancies are compensated either by computing anharmonic corrections explicitly or by introducing scalar field or even by direct scaling of the calculated wavenumbers with a proper scaling factor. The comparison of the scaled wavenumbers with experimental values reveals that the B3LYP method shows very good agreement with the experimentally observed spectra. The computed IR and Raman spectral intensities were used to convolute all the predicted vibrational modes using a pure Lorentzian line shape with a FWHM bandwidth of 5 cm^{-1}, to simulate the spectra given in Figs 2 and 3 with experimental spectra. The vibrational band assignments were made by the help of potential energy distribution (PED) using VEDA program. The experimental and scaled calculated wavenumbers and complete assignments are presented in Table 2.

5.2.1 C-H vibrations

The aromatic C-H ring stretching vibrations are normally found between[16] 3100 and 3000 cm^{-1}. The calculated frequencies which lie in the range 3116, 3082, 3068, 3067, 3058, 3053, 3044, and 3025 cm^{-1} are assigned to the three C-H stretching vibrations of the title compound in 2BNP2E and their experimental counterpart appear in the range 3126(s), 3074(s) cm^{-1} of the IR spectrum and 3093(s), 3059(vs), 3043(w), 3036(s), 3011(w) cm^{-1} of the Raman spectrum.

5.2.2 Methylene group vibrations

The asymmetric stretching modes of the CH_2 and CH_3 group are higher than the symmetric stretching modes[17,18]. The C-H stretching vibrations of the methylene group are at lower frequencies then those of the aromatic C-H ring stretching. The asymmetric CH_2 stretching vibration is generally observed in the region 3000-2900 cm^{-1}, while the CH_2 symmetric stretching will appear between[19,20] 2900-2800 cm^{-1}. The band observed at 2999(m), 2922(m) cm^{-1} in FTIR and band observed at 2987(vs), 2931(vs) in FT-Raman is due to CH_2 stretching. The calculated scaled wavenumbers is 3003, 3002, 2893 cm^{-1} are assigned to CH_2 asymmetric and symmetric vibrations contributing 97, 97 and 93% to PED

5.2.3 C-N vibrations

The ring C-C and C-N stretching vibrations occur in the wide range from[21] 1640-900 cm^1. Silverstein *et al.*[22] have assigned C-N stretching absorption in the region 1342-1266 cm^{-1}. The identification of C-N stretching frequencies was a rather difficult task since the mixing of vibrations was possible in this region[23,24]. In this study, the bands observed at 1489(vs) cm^{-1} in FTIR spectrum and 1491(s), 1202(w), 1181(s), 948(w) cm^{-1} in Raman spectrum have been assigned to C-N stretching vibrations of the title compound. The C-N stretching vibration was moderately lowered wavenumber, which may be due to the mass effect around nitrogen atom[25].

5.2.4 C-C vibrations

The benzene possesses six stretching vibrations of which the four with highest wave numbers occurring

Table 2 — Calculated vibrational frequencies (cm^{-1}) assignments of 2BNP2E based on B3LYP/6-311++G(d,p) basis set (*Contd*.).

Mode number	Experimental wave number (cm^{-1})		Theoretical wave number (cm^{-1})		I_{IR}[c]	I_{RAMAN}[d]	Assignments (PED)[a,b]
	FTIR	FT-Raman	Unscaled	scaled			
93	-	3485(w)	3624	3483	3	6	γ NH(100)
92	3126(s)	-	3243	3116	1	3	γ CH(99)
91	3074(s)	-	3207	3082	1	10	γ CH(99)
90	-	3093(s)	3193	3068	1	2	γ CH(95)
89	-	-	3192	3067	0	3	γ CH(91)
88	-	-	3191	3066	5	18	γ CH(98)
87	-	3059(vs)	3182	3058	2	3	γ CH(91)
86	-	3043(w)	3177	3053	5	6	γ CH(68)
85	-	3036(s)	3167	3044	0	5	γ CH(98)
84	-	3011(w)	3147	3025	3	2	γ CH(90)
83	2999(m)	-	3125	3003	3	5	γ_{as} CH_2(97)
82	-	2987(vs)	3124	3002	9	8	γ_s CH_2(97)
81	2922(m)	2931(vs)	3010	2893	31	18	γ_s CH_2(93)
80	1681(vs)	1664(vs)	1723	1656	77	87	γ OC(69)
79	1606(vs)	1621(w)	1680	1614	5	28	γ OC(69) + γ CC(18)+ βHCC(11)
78	-	1592(vs)	1646	1582	6	100	γ CC(93)
77	-	-	1641	1577	20	83	γCC (18)+ γNC(27)
76	-	1569(w)	1639	1575	1	1	γCC(38)+ βCCC(10)
75	1537(vs)	1547(vs)	1632	1568	14	3	γCC(46)+ βHNC(43)
74	1489(vs)	1491(s)	1554	1493	99	26	γNC(28)+ βHNC(43)
73	-	1479(w)	1540	1480	8	2	sis HCH(77)
72	-	1468(m)	1525	1466	9	8	βHCC(84)
71	1449(vs)	1447(s)	1521	1462	80	0	βHCC(57) +βHCH(12)
70	1393(vs)	1409(w)	1470	1412	11	1	γCC(46)+ βHCC(28)+ βCCC(12)
69	-	-	1465	1408	33	9	βHCC(40)
68	1370(vs)	1372(vs)	1427	1371	0	2	τHCOC(65)
67	-	1348(m)	1389	1335	33	37	γCC(28)+ wag HCC(34)
66	1313(vs)	1315(vs)	1355	1302	0	0	γCC(38)+ wag HCC(60)
65	1291(vs)	1293(vs)	1346	1294	6	7	γCC(42)+ twist HCC(56)
64	-	1274(w)	1338	1286	36	17	γCC(23)+ twist HCC(18)
63	1259(vs)	1261(s)	1305	1254	18	23	γCC(16)+ γHCC(51)
62	-	1237(vs)	1293	1242	36	17	γCC(23)+ βHCC(72)
61	-	-	1273	1224	16	8	γCC(23)+ βHCC(38)
60	-	1202(w)	1260	1211	17	31	γCC(11)+ γNC(27) βHNC(43)
59	-	1181(s)	1236	1188	100	14	γCN(28)+ γCC(21)
58	1169(s)	1171(vs)	1219	1172	8	7	βHCO(31)+ τHCOC(43)
57	-	1162(s)	1202	1155	1	1	βHCC(84)
56	-	-	1201	1154	6	21	βHCO(31) +βHCC(28)
55	-	-	1182	1136	0	1	βHCC(58)
54	1117(s)	1119(s)	1163	1118	4	0	γCC(23)+ βHCC(62)
53	1089(vs)	1091(vs)	1142	1097	2	0	βHCO(31))+ τHCOC(42) + τCOCC(16)

(*Contd*.)

Table 2 — Calculated vibrational frequencies (cm^{-1}) assignments of 2BNP2E based on B3LYP/6-311++G(d,p) basis set (*Contd*.).

Mode number	Experimental wave number (cm^{-1})		Theoretical wave number (cm^{-1})		I_{IR}[c]	I_{RAMAN}[d]	Assignments (PED)[a,b]
	FTIR	FT-Raman	Unscaled	scaled			
52	-	1068(w)	1111	1068	3	2	γCC(38)+ βHCC(42)
51	-	-	1109	1066	10	11	βCCC(62)
50	1037(vs)	1022(m)	1058	1016	34	0	γOC(40)+ βCOC(17)+ βOCC(13)
49	1009(vs)	1010(s)	1051	1010	2	1	γCC(46)+ βHCC(21)+ τHCCN(25)
48	-	972(vs)	1013	974	0	4	βCCC(63)
47	967(s)	956(w)	1002	963	6	3	τHCCN(25)+ τHCCC(53)
46	-	-	1001	962	4	3	τHCCN(12)+ τHCCC(45) + τCCCC(25)
45	-	948(w)	985	947	1	3	γNC (28)+ γCC(21)
44	929(s)	937(w)	976	938	0	0	τHCCC(96)
43	-	-	948	911	0	1	γOC(40)
42	-	910(w)	945	908	10	1	γOC(40)+ βCOC(17)+ βOCC(13)
41	-	903(w)	941	904	1	0	τHCCC(72) + τCCCC(22)
40	-	892(w)	916	880	2	0	τHCCC(96)
39	-	870(w)	895	860	2	4	τHCCN(25)+ τHCCC(62) + τCCCN(11)
38	-	846(vs)	871	837	3	2	γCC(23)+ βCCN(18)+ τHCCC(23)
37	828(vs)	-	861	827	6	0	τHCCC(23)+OutONCC(34)
36	-	821(s)	841	808	0	0	τHCCC(84)
35	-	795(w)	830	798	3	2	γCC(56)+ γOC(22)
34	785(s)	788(w)	823	790	7	0	τHCCC(80)
33	-	-	804	773	2	1	γOC(21)+ βCCC(22)
32	750(s)	742(w)	767	738	13	0	τHCCC(35) + τCCCC(11)+ OutNCCC(47)
31	-	709(vs)	743	714	0	0	βCOC(17)
30	706(s)	-	730	701	1	0	τCCCC(45)+ OutONCC(34)+ OutOCCC(14)
29	-	694(w)	721	693	0	1	τCCCC(40)
28	-	683(w)	704	677	8	0	τHCCC(65) + τCCCC(11)
27	-	662(w)	703	675	1	0	OutONCC(34)
26	626(m)	632(vs)	642	617	0	0	γCC(38)+ βCCC(14)
25	607(m)	607(w)	633	608	0	0	βCCC(42)
24	-	-	605	581	1	0	τCCCC(48)+ OutOCCC(13)
23	-	-	574	552	3	0	τHNCC(14)
22	-	-	555	533	7	0	βOCC(24)+ τHNCC(14)
21	-	518(w)	548	527	8	0	τHNCC(14)
20	506(s)	483(w)	518	498	4	0	τHCCC(46) + τCCCC(11)+ OutNCCC(37)
19	449(s)	452(s)	459	441	0	0	βCCC(24)+βOCC(16)
18	-	428(w)	430	413	1	0	τCCCC(44)+ OutOCCC(13)
17	-	414(w)	417	401	0	0	τHCCC(65) + τCCCC(32)
16	-	389(s)	397	381	2	0	βNCC(28)+βCCN(18)
15	-	356(vs)	360	346	1	0	τCCCC(22)+ OutOCCC(14)

(*Contd*.)

Table 2 — Calculated vibrational frequencies (cm^{-1}) assignments of 2BNP2E based on B3LYP/6-311++G(d,p) basis set.

Mode number	Experimental wave number (cm^{-1})		Theoretical wave number (cm^{-1})		I_{IR}[c]	I_{RAMAN}[d]	Assignments (PED)[a,b]
	FTIR	FT-Raman	Unscaled	scaled			
14	-		347	333	0	0	γNC(10)+ βOCC(10)+ βCCC(19)+βCNC(29)+ βNCC(24)
13	-	301(s)	305	293	2	0	βOCC(24)+βCCC(14)
12	-	270(vs)	261	251	0	0	τCCCC(15)+ OutOCCC(13)
11	-	-	245	236	0	0	τCCCC(42)+ OutOCCC(13)
10	-	-	199	191	0	0	τCCCC(40)
9	-	168(s)	171	164	2	0	βCNC(29)+βNCC(28)
8	-	153(vs)	154	148	1	0	βCCC(27)+βCCN(18)
7	-	-	128	123	3	0	τHCOC(32) + τCOCC(16)
6	-	-	114	110	1	0	βCCC(14)+τCCCN(24) +τCCCC(13) + τCCNC(40)
5	-	-	83	80	0	0	τCCCN(24) +τCCCC(22) + τCNCC(13)+ + τCCNC(40)
4	-	-	49	47	0	0	τCCCC(22) +τCNCC(51)
3	-	-	38	36	0	0	βCCC(23)+βCCN(18)+ τCCCC(13)
2	-	-	26	25	0	0	τCNCC(51) +τCCCC(13) + τCCNC(11)
1	-	-	14	14	0	0	τCCCN(24) +τCCCC(68)

[a]γ-stretching,γ_a-symmetrical stretching,γ_{as}-asymmetrical stretching, β- bending , wag-wagging, twist-twisting, sis- scissoring, τ-torsion, vs-very strong, s- strong, m-medium, w-weak.
[b]scaling factor : 0.961 for B3LYP/6-311+G(d,p).
[c]Relative absorption intensities normalized with highest peak absorption equal to 100.
[d]Relative Raman intensities normalized to 100.

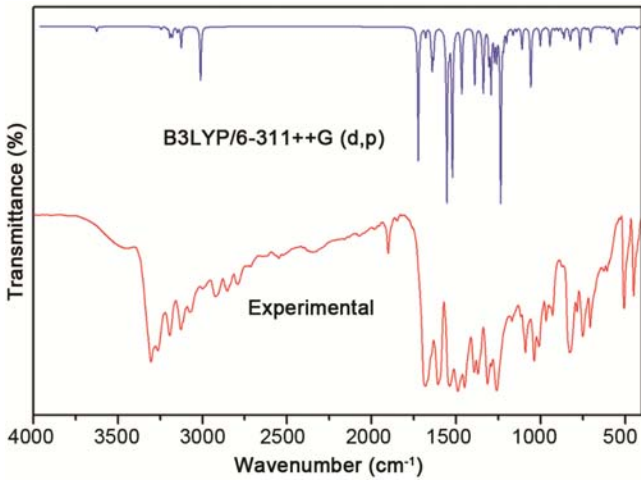

Fig. 2 — Experimental and theoretical FT-IR spectra of 2BNP2E.

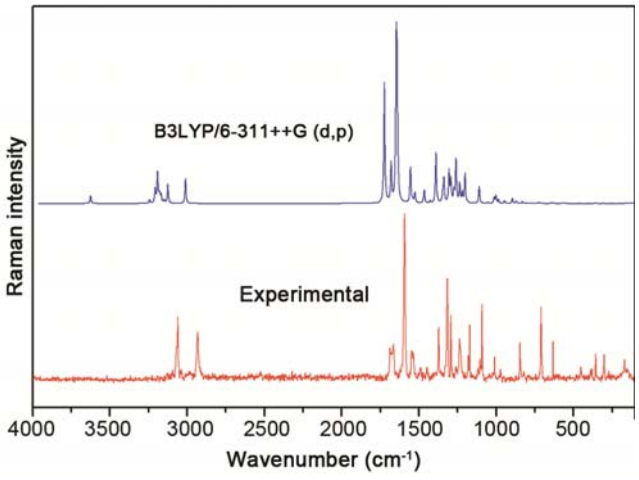

Fig. 3 — Experimental and theoretical FT-Raman spectra of 2BNP2E.

near 1650–1400 cm^{-1} are good group vibrations[26]. With heavy substituents, the bonds tend to shift to somewhat lower wave numbers and greater the number of substituents on the ring, broader the absorption regions. In the title molecule, the bands observed in FTIR and FT-Raman at 1606(vs), 1537(vs), 1393(vs), 1313(vs), 1291(vs), 1259(vs), 1009(vs), 626(vs) cm^{-1} and 1621(w), 1592(vs), 1569(w), 1547(vs), 1409(w), 1348(m), 1315(vs), 1293(vs), 1261(s), 1237(vs), 1181(s), 1117(s), 1010(s), 846(vs), 632(vs) cm^{-1} respectively have been

assigned to C-C stretching vibrations are due to the substituents in benzene ring. The calculated C-C stretching vibrations using B3LYP/6-311++G (d,p) shows a very good agreement with the experimental values is given in Table 2.

5.3 Hyperpolarizability calculation

NLO is at the future of current research because it provides the key functions of frequency shifting, optical modulation, optical switching, optical logic, and optical memory for the emerging technologies in areas such as telecommunications, signal processing, and optical interconnections[27,28]. In discussing NLO properties, the polarization of the molecule by an external radiation field is often approximated as the creation of an induced dipole moment by an external electric field. The first hyperpolarizability (β_0) of this molecular system is calculated using B3LYP/6-311++G (d,p) method, based on the finite field approach. The complete equations for calculating the magnitude of total static dipole moment μ, the mean polarizability α_0, the anisotropy of the polarizability $\Delta\alpha$ and the mean first polarizability β_0, using the *x*, *y*, *z* components from Gaussian 03W output are as follows:

$$\mu_{tot} = (\mu_x^2 + \mu_y^2 + \mu_z^2)^{1/2} \quad \ldots (1)$$

$$\alpha_0 = (\alpha_{xx} + \alpha_{yy} + \alpha_{zz})/3 \quad \ldots (2)$$

$$\Delta\alpha = 2^{-1/2}[(\alpha_{xx} - \alpha_{yy})^2 + (\alpha_{yy} - \alpha_{zz})^2 + [(\alpha_{zz} - \alpha_{xx})^2 6\,\alpha^2 xx]^{1/2} \quad \ldots (3)$$

$$\beta_0 = (\beta_x^2 + \beta_y^2 + \beta_z^2)^{1/2} \quad \ldots (4)$$

and

$$\beta_x = \beta_{xxx} + \beta_{xyy} + \beta_{xzz} \quad \ldots (5)$$

$$\beta_y = \beta_{yyy} + \beta_{xxy} + \beta_{yzz} \quad \ldots (6)$$

$$\beta_z = \beta_{zzz} + \beta_{xxz} + \beta_{yyz} \quad \ldots (7)$$

The calculated hyperpolarizability values of 2BNP2E are given in Table 3. Urea is one of the prototypical molecules used in the study of the NLO properties of molecular systems and frequently used as a threshold value for comparative purposes. The first order hyperpolarizability of 2BNP2E with B3LYP/6-311++G(d,p) basis set is 13.586×10^{-30} thirty six times greater than the value of urea ($\beta_o = 0.372\times10^{-30}$ esu).

5.4 Frontier molecular orbital (FMO) analysis

The electronic absorption corresponds to the transition from the ground state to the first excited state and is mainly described by one electron-excitation from the highest occupied molecular orbital (HOMO) to the lowest unoccupied molecular orbital (LUMO). The HOMO as an electron donor represents the ability to donate the electron, while LUMO as an electron acceptor represents the ability to obtain the electron. Both HOMO and LUMO are the main orbital that take part in chemical stability[29]. The energy values of LUMO and HOMO and their energy gap reflect the chemical activity of the molecule. Therefore, while the energy of the HOMO is directly related to the ionization potential, LUMO energy is directly related to the electron affinity. Energy difference between HOMO and LUMO orbital is called as energy gap that is an important stability for structure[30]. The atomic orbital compositions of the frontier molecular orbital are sketched in Fig. 4.

Considering the chemical hardness, large HOMO-LUMO energy gap means a hard molecule and small HOMO-LUMO energy gap means a soft molecule[31]. One can also relate the stability of the molecule to hardness, which means that the molecule with least HOMO-LUMO gap is more reactive. Table 4 lists the calculated values HOMO- LUMO of the first ionization potentials, HOMO, LUMO and energy gaps of 2BNP2E. The energy gap between the HOMO and the LUMO molecular orbital is a critical parameter in determining molecular electrical transport properties because it is a measure of electron conductivity. The lowest unoccupied molecular orbital (LUMO) energy is -2.0610 eV and the highest occupied molecular orbital (HOMO) energy is -6.0681 eV. Al-Wabli *et al.*[32] reported HOMO-LUMO energy gap of N-[(1E)-1-(2H-1,3-Benzodioxol-5-yl)-3-(1H-imidazol-1-yl)propylidene]-hydroxylamine is

Table 3 — The values of calculated dipole moment μ (D), polarizability (α_0), first order hyperpolarizability (β_{tot}) components of 2BNP2E

Parameters	B3LYP/6-311++G(d,p)	Parameters	B3LYP/6-311++G(d,p)
μ_x	3.1335	β_{xxx}	-1113.4492
μ_y	-0.02082	β_{xxy}	14.97135
μ_z	-0.02233	β_{xyy}	-396.3578
μ(D)	3.1336	β_{yyy}	-517.9374
α_{xx}	370.6941	β_{zxx}	61.12301
α_{xy}	-75.6896	β_{xyz}	63.29286
α_{yy}	219.6819	β_{zyy}	-87.39013
α_{xz}	-22.21198	β_{xzz}	14.1393
α_{yz}	10.24914	β_{yzz}	21.60713
α_{zz}	107.45307	β_{zzz}	92.3827
α_0 (e.s.u)	3.4473×10^{-23}	β_{tot} (e.s.u)	13.586×10^{-30}
$\Delta\alpha$(e.s.u)	10.1010×10^{-23}		

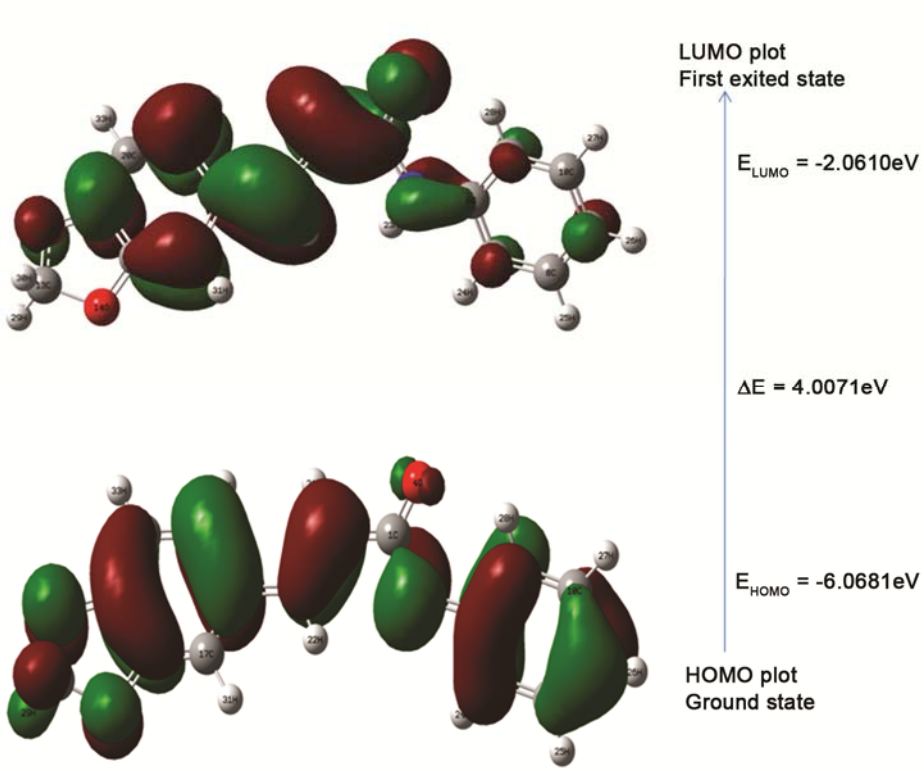

Fig. 4 — Highest occupied and lowest unoccupied molecular orbital of 2BNP2E obtain with B3LYP/6-311++G(d,p) method.

Table 4 — Calculated energy values of title compound by B3LYP/6-311++G(d,p) method.

Basis set	B3LYP/6-311++G(d, p)
E_{Homo} (eV)	-6.0681
E_{Lumo} (eV)	-2.0610
Ionization potential	6.0681
Electron affinity	2.061
Energy gap (eV)	4.0071
Electronegativity	4.06455
Chemical potential	-4.06455
Chemical hardness	2.00355
Chemical softness	0.249557
Electrophilicity index	4.122824

found to be 4.630 eV. According to DFT calculation, the frontier orbital energy gap of 2BNP2E is found to be 4.0071 eV. Hence, the energy gap of title compound 2BNP2E is low. This smaller energy gap of HOMO–LUMO explains the eventual charge transfer occurs within the molecule, which influences its high polarizability and biological activities.

5.5 NBO analysis

NBO analysis provides the most accurate possible 'natural Lewis structure' picture of φ, because all the orbital details are mathematically chosen to include the highest possible percentage of the electron density. A useful aspect of the NBO method is that it gives information about interactions in both filled and virtual orbital spaces that could enhance the analysis of intra- and intermolecular interactions. The second-order Fock matrix was carried out to evaluate the donor-acceptor interactions in NBO analysis[33]. For each donor (I) and acceptor (j), the stabilization energy $E(2)$ associated with the delocalization i, j estimated as:

$$E_2 = \Delta E_{ij} = q_i[(F(i,j)^2)/(E_i\text{-}E_j) \quad \ldots (8)$$

where q_i is the donor orbital occupancy, E_i and E_j are diagonal elements and $F(i,j)$ is the off diagonal NBO Fock matrix elements.

NBO analysis provides an efficient method for studying intra and intermolecular bonding and interaction among bonds, and also provides a convenient basis for investigation charge transfer or conjugative interactions in molecular system[34].

The strong intramolecular hyper conjugative interaction of the σ and π electrons of C-C to the anti C-C bond of the ring leads to stabilization of some part of the ring as evident from Table 5. The strong intramolecular hyperconjugative interaction of

Table 5 — Second order perturbation theory analysis of Fock matrix in NBO basis for 2BNP2E (*Contd*.).

Donor (*i*)	Type	ED/e	Acceptor (*i*)	Type	ED/e	[a]*E*(2) (kJ mol^{-1})	[b]*E*(*J*)-*E*(*i*) (a.u.)	[c]*F*(*I*,*j*) (a.u.)
C_1-C_2	σ	1.9726	C_1-N_5	σ*	0.0673	4.610	1.350	0.071
			C_2-C_3	σ*	0.0201	4.590	1.360	0.071
C_1-O_4	σ	1.9873	C_1-C_2	σ*	0.0408	4.330	1.660	0.076
C_1-O_4	π	1.9571	C_2-C_3	π*	0.1673	7.770	0.400	0.052
C_1-N_5	σ	1.9799	N_5-C_6	σ*	0.0349	6.180	1.540	0.088
C_2 -C_3	σ	1.9716	C_3-C_{18}	σ*	0.0315	5.580	1.380	0.078
			C_{17}-C_{18}	σ*	0.0301	4.700	1.380	0.072
C_2-C_3	π	1.8224	C_1-O_4	π*	0.4124	29.110	0.310	0.090
			C_{18}-C_{19}	π*	0.4299	15.860	0.330	0.069
C_2-H_{21}	σ	1.9679	C_1-N_5	σ*	0.0673	4.710	1.140	0.066
			C_3-H_{22}	σ*	0.0259	5.410	0.910	0.063
C_3-C_{18}	σ	1.9643	C_2-C_3	σ*	0.0201	4.730	1.370	0.072
			C_{17}-C_{18}	σ*	0.0301	7.360	1.390	0.090
			C_{18}-C_{19}	σ*	0.0356	7.250	1.370	0.089
C_3-H_{22}	σ	1.9676	C_2-H_{21}	σ*	0.0191	4.490	0.960	0.059
			C_{18}-C_{19}	σ*	0.0356	4.870	1.180	0.068
N_5-C_6	σ	1.9790	C_1-N_5	σ*	0.0673	5.640	1.520	0.084
			C_6-C_7	σ*	0.0313	4.190	1.580	0.073
			C_6-C_{11}	σ*	0.0346	4.260	1.590	0.074
N_5-H_{23}	σ	1.9777	C_1-O_4	σ*	0.0206	5.220	1.310	0.074
C_6-C_7	σ	1.9627	C_6- C_{11}	σ*	0.0346	8.800	1.400	0.099
			C_7-C_8	σ*	0.0185	4.890	1.400	0.074
C_6-C_7	π	1.6446	C_8-C_9	π*	0.3631	23.370	0.320	0.078
			C_{10}-C_{11}	π*	0.3631	18.510	0.340	0.071
C_6-C_{11}	σ	1.9521	N_5-C_6	σ*	0.0349	5.370	1.340	0.076
			N_5-H_{23}	σ*	0.0409	5.420	1.010	0.066
			C_6-C_7	σ*	0.0313	8.650	1.370	0.098
C_7-C_8	σ	1.9730	C_6-C_7	σ*	0.0313	5.190	1.380	0.076
C_8-C_9	π	1.6689	C_6-C_7	π*	0.4331	20.010	0.300	0.071
			C_{10}-C_{11}	π*	0.3631	21.450	0.320	0.075
C_{10}-C_{11}	π	1.6455	C_6-C_7	π*	0.4331	26.570	0.290	0.080
			C_8-C_9	π*	0.3631	22.870	0.300	0.074
C_{13}-O_{14}	σ	1.9838	C_{15}-C_{17}	σ*	0.0285	8.150	1.490	0.099
C_{15}-C_{16}	σ	1.9634	C_1-C_{17}	σ*	0.0285	7.990	1.380	0.094
			C_{16}-C_{20}	σ*	0.0301	8.080	1.380	0.094
C_{15}-C_{17}	π	1.6857	C_{16}-C_{20}	π*	0.4167	21.580	0.310	0.075
			C_{18}-C_{19}	π*	0.4299	21.170	0.340	0.078
C_{16}-C_{20}	σ	1.9652	C_{19}-H_{32}	σ*	0.0188	24.070	5.330	0.321
			C_{15}-C_{17}	π*	0.3953	22.190	0.320	0.076
			C_{18}-C_{19}	π*	0.4299	20.720	0.340	0.076
C_{18}-C_{19}	π	1.6188	C_2-C_3	π*	0.1673	18.430	0.300	0.070
			C_{15}-C_{17}	π*	0.3953	21.610	0.300	0.072
			C_{16}-C_{20}	π*	0.4167	23.220	0.290	0.074
C_{19}-C_{20}	σ	1.9714	C_{19}-C_{20}	σ*	0.0154	18.050	3.940	0.239
			C_{19}-H_{32}	σ*	0.0188	15.830	5.310	0.259
C_{20}-H_{33}	σ	1.9753	C_{19}-C_{20}	σ*	0.0154	10.030	3.710	0.173
			C_{19}-H_{32}	σ*	0.0188	65.570	5.080	0.516
O_4	LP(1)	1.9530	C_{11}-H_{28}	σ*	0.0588	13.700	1.140	0.112

(*Contd.*)

Table 5 — Second order perturbation theory analysis of Fock matrix in NBO basis for 2BNP2E.

Donor (*i*)	Type	ED/e	Acceptor (*i*)	Type	ED/e	[a]*E*(2) (kJ mol^{-1})	[b]*E*(*J*)-*E*(*i*) (a.u.)	[c]*F*(*I*,*j*) (a.u.)
O_4	LP(2)	1.8843	C_1-C_2	σ*	0.0408	14.780	0.900	0.105
			C_1-N_5	σ*	0.0673	16.410	0.910	0.110
			C_{11}-H_{28}	σ*	0.0588	20.930	0.800	0.117
N_5	LP(1)	1.6145	C_1-O_4	π*	0.4124	86.500	0.300	0.144
			C_6-C_7	π*	0.4331	52.030	0.330	0.119
O_{12}	LP(2)	1.8038	C_{16} -C_{20}	π*	0.4167	43.540	0.400	0.125
O_{14}	LP(2)	1.8156	C_{15}-C_{17}	π*	0.3953	43.910	0.400	0.125

[a]$E^{(2)}$ means energy of hyper conjugative interaction (stabilization energy).
[b]Energy difference between donor and acceptor *i* and *j* NBO orbitals.
[c]$F(i,j)$ is the Fock matrix element between *i* and *j* NBO orbitals.

σ (C_6-C_7) distributes to σ*(C_6- C_{11}), and σ*(C_7-C_8) of the ring. On the other hand, side the π(C_6-C_7) in the ring conjugate to the anti-bonding orbital of π*(C_8-C_9) and π*(C_{10}-C_{11}) which leads to strong delocalization of 23.370, and 18.510 kJ/mol, respectively. The most important interaction energy, related to the resonance in the molecule is electrons donating from LP (1) N_5 donor to antibonding acceptor π*(C_1-O_4) and π* (C_6-C_7) with large stabilization energy of 86.50, 52.03 kJ/mol as shown in Table 5. A loan pair of the nitrogen acts on electronegative atom. Basically, the electronegative atom is most involved donor-acceptor interaction.

5.6 Molecular electrostatic potential

The molecular electrostatic potential (MEP) is the most useful electrostatic property to study the relation between the structure and activity. The MEP has been also employed as an information tool of chemistry to describe different physical and chemical features, including non-covalent interactions in complex biological system. The electrostatic potential created by the nuclei and electrons of a molecule in the surrounding space is well established as a guide to the interpretation and prediction of molecular behavior. It has been shown to be a useful tool in studying both electrophilic and nucleophilic processes[35-37], in particular, to be well suited for studies that involve the identification of key features necessary for the ‘‘recognition’’ of one molecule by molecular electrostatic potential (MEP) which is related to the electronic density and is a very useful descriptor in understanding sites for electrophilic attack and nucleophilic reactions as well as hydrogen bonding interactions[38-40]. At any given point $r(x,y,z)$ in the vicinity of a molecule, MEP $V(r)$ is defined in terms of the interaction energy between the electrical energy generated from the molecule electrons and nuclei and a positive test charge[41,42] (a proton). At point r, the MEP, $V(r)$ is given by:

$$V(r) = Z_A / (R_A - r) \quad \ldots (9)$$

where, $V(r)$ is the electron density at r , Z_A is the charge on nucleus a located at R_A. The first term is due to the nuclear charge, the second, to the electronic distribution.

MEP surface diagram is used to understand the reactive behavior of a molecule, in that negative regions can be regarded as potential electrophilic sites, whereas the positive regions are nucleophilic centers. To predict reactive sites for electrophilic attack for the title compound, MEP was calculated by B3LYP /6-311++G(d,P) optimized geometry. Molecular electrostatic potential mapping is very useful in the investigation of the molecular structure with its physiochemical property relationships[43,44]. The negative (red) regions, of MEP were related to electrophilic reactivity and the positive (blue) ones to nucleophilic reactivity shown in Fig. 5. As easily can be seen in figure, this molecule has two possible sites for electrophilic attack. For the title compound, negative regions were calculated the MEP value around O is more negative than that of H atom. The contour map of electrostatic potential of 2BNP2E has been constructed by the DFT method and is shown in Fig. 6. It also confirms the different negative and positive potential sites of the molecule in accordance with the total electron density surface.

5.7 Thermodynamic properties

On the basis of vibrational analysis at B3LYP/6-311++G(d,p) level, the standard statistical thermodynamic functions such as heat capacity $C^0_{p,m}$, entropy S^0_m and enthalpy changes H^0_m for the title

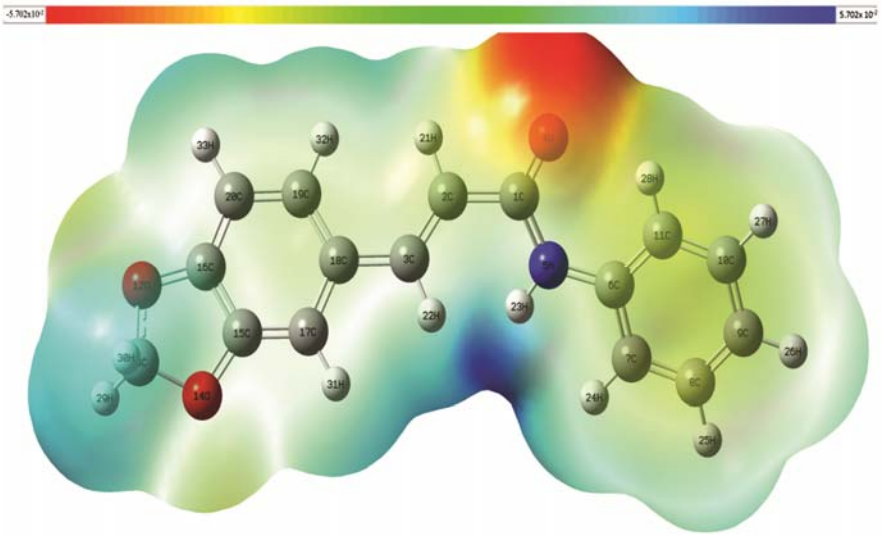

Fig. 5 — Molecular electrostatic potential of 2BNP2E calculated at B3LYP/6-311++G(d,p) basis set.

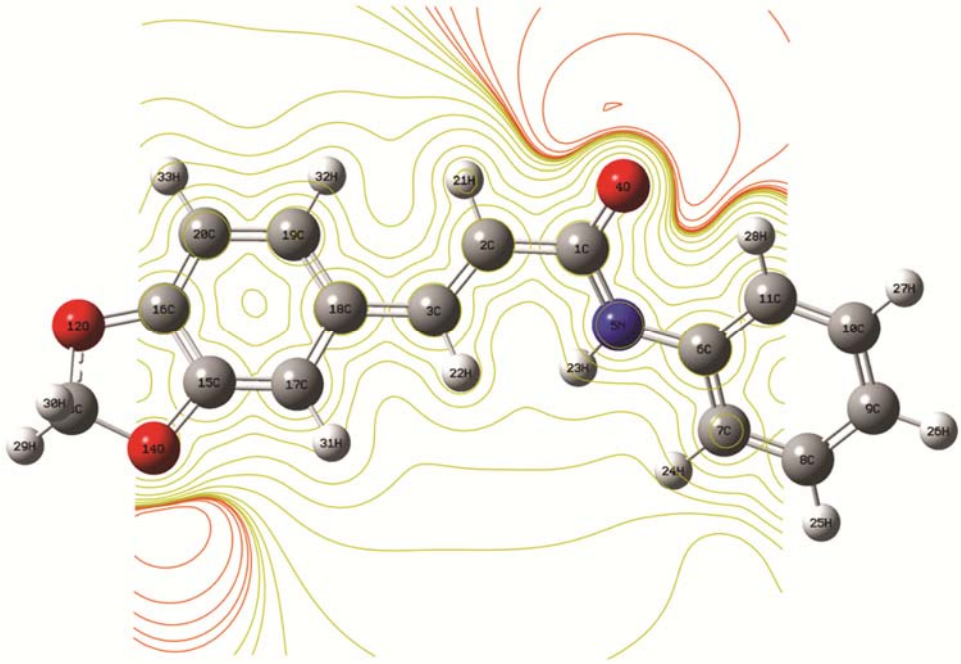

Fig. 6 — The contour map of electrostatic potential of the total density of 2BNP2E.

compound were calculated using Perl script[45] THERMO.PL and are listed in Table 6. From Table 6, it can be observed that these thermodynamic functions are increasing with temperature ranging from 100 to 1000 K due to the fact that the molecular vibrational intensities increase with temperature[46,47]. The correlation equations between heat capacity, entropy, enthalpy changes and temperatures are built-in by quadratic formulas. The fitting factors (R^2) for these thermodynamic properties are 0.9986, 0.9999 and 0.9993, respectively. The corresponding fitting equations are as follow and the correlation graphs of those are represented in Fig. 7:

$$C^0_{p,m} = 4.9219 + 1.0579T - 4.4018 \times 10^{-4}T^2 \quad (R^2 = 0.9986) \quad \ldots (10)$$

$$S^0_m = 273.317 + 1.0726T - 2.2348 \times 10^{-4}T^2 \quad (R^2 = 0.9999) \quad \ldots (11)$$

$$H^0_m = - 11.0658 + 0.1148T + 2.898 \times 10^{-4}T^2 \quad (R^2 = 0.9993) \quad \ldots (12)$$

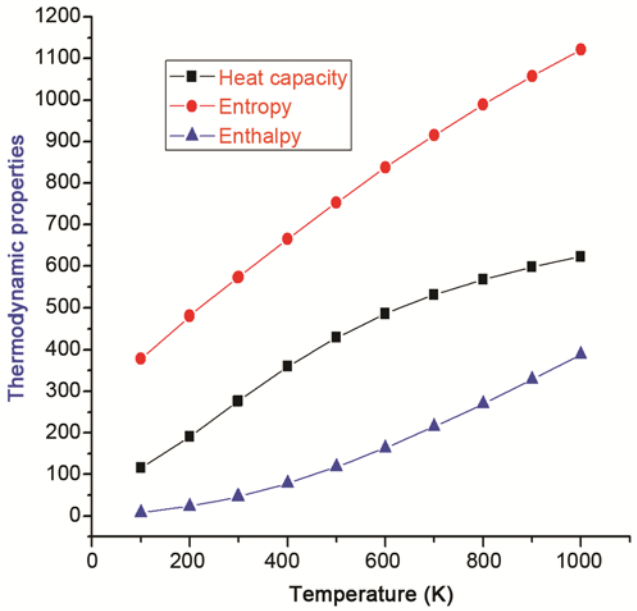

Fig. 7 — Correlation graphic of heat capacity, entropy, enthalpy and temperature for 2BNP2E.

Table 6 — Temperature dependence of thermodynamic properties of 2BNP2E at B3LYP /6-311++G(d,P).

T (K)	$C^0_{p,m}$ (J/ mol K)	S^0_m (J/ mol K)	H^0_m (kJ/ mol)
100	116.29	378.21	7.89
200	190.59	480.75	23.11
298.15	275.27	572.46	45.93
300	276.88	574.17	46.44
400	359.8	665.43	78.36
500	429.79	753.5	117.96
600	486.08	837.02	163.86
700	531.18	915.47	214.8
800	567.77	988.87	269.81
900	597.92	1057.54	328.14
1000	623.09	1121.87	389.23

These equations could be used for the further studies on the title compound. They can be used to compute the other thermodynamic energies according to relationships of thermodynamic functions and estimate directions of chemical reactions according to the second law of thermodynamics in thermochemical field[48]. All thermodynamic calculations were done in gas phase and they could not be used in solution.

6 Conclusions

In this work, we have performed the experimental and theoretical vibrational analysis of 2BNP2E. The molecular geometry, vibrational frequencies, FTIR and FT-Raman spectra of the molecule in the ground state are calculated by using DFT (B3LYP) method 6-311++G(d,p) basis set. The vibrational wavenumbers are calculated and the complete assignments are performed on the basis of the PED of the vibrational modes. The results are compared with experimental FT-IR and FT-Raman spectra. The correlation graphic is plotted to see the harmony between the calculated and experimental wavenumbers and the graphic showed a very good coherence with FTIR results. Nonlinear optical (NLO) behaviour of the title molecule has been investigated by the dipole moment, the polarizability and the first order hyperpolarizability. HOMO-LUMO gap is calculated as 4.0071 eV. Additionally, the thermodynamic and the electronic properties of the studied compound are calculated. Using NBO analysis the stability of the molecule arising from hyper-conjugative interaction and charge delocalization has been analyzed. Also, thermodynamic properties in the range from 100 to 1000 K are obtained. As a result, this study made for 3,4-PDCA gave us a full work related to the geometry, vibrational properties (based on FTIR, FT-Raman), NLO, HOMO-LUMO, NBO, MEP and thermodynamic properties.

References

1 Hamel E, *Med Res Rev*, 16 (1996) 207.
2 Batra J K, Jurd L & Hamel E, *Mol Pharmacol*, 27 (1985) 94.
3 Jurd L, Narayanan V L & Paull K D, *J Med Chem*, 30 (1987) 1752.
4 Yokota S, Kitahara M & Nagata K, *Cancer Res*, 60 (2000) 2942.
5 Xia Y, Yang Z, Xia P, Bastow K F, Nakanishi Y & Lee K, *Bioorg Med Chem Lett*, 10 (2000) 699.
6 Moreira M, Lima Leite A C, Ferreira P M P, Costa P M D, Costa Lotufo L V, Moraes M O D, Brondani D J & Pessoa C, *Eur J Med Chem*, 42(2007) 351.
7 Chimirri A, Grasso S, Monforte A M & Rao A, Zappala M, *Farmaco*, 51 (1996) 125.
8 Grasso S, Micale N, Monforte A M, Monforte P & Zappala M, *Eur J Med Chem*, 35 (2000) 1115.
9 Micale N, Zappala M & Grasso S, *Farmaco*, 57 (2002) 854.
10 Frisch J, Trucks G W, Schlegel H B, Scuseria G E, Robb M A, Cheeseman J R, Scalmani G, Barone V, Mennucci B, Petersson A, Nakatsuji H, Caricato M, Li X, Hratchian H P, Izmaylov A F, Bloino J, Zheng G, Sonnenberg J L, Hada M, Ehara M K, Toyota K, Fukuda R, Hasegawa J, Ishida M, Nakajima T, Honda Y, Kitao O, Nakai O, Vreven T, Montgomery J A, Peralta J E, Ogliaro F, Bearpark M, Heyd J J, Brothers E, Kudin K N, Staroverov V N, Keith T, Kobayashi R, Normand J Raghavachari K, Rendell A, Burant J C, Iyengar S S, Tomasi J, Cossi M, Rega N, Millam J M, Klene M, Knox J E, Cross J B, Bakken V, Adamo C, Jaramillo J, Gomperts R, Stratmann R E,

Yazyev O, Austin A J, Cammi R, Pomelli C, Ochterski J W, Martin R L, Morokuma K, Zakrzewski G, Voth G A, Salvador P, Dannenberg J J, Dapprich S, Daniels A D, Farkas O, Foresman J B, Ortiz J V, Cioslowski J & Fox D J, *Gaussian, Inc*, (Wallingford CT), 2010.

11 Schlegel H B, *J Comput Chem*, 3 (1982) 214.

12 Foresman J B & Frisch A, *Exploring chemistry with electronic structure methods*, (Gaussian Inc: Pittsburgh), 1996.

13 Jomroz M H, *Vibrational energy distribution analysis*, (VEDA:Warsaw), 2004.

14 Glendening E D, Reed A E, Carpenter J E, Weinhold F, *NBO 3.0 program manual,* Theoretical Chemistry Institute and Department of Chemistry, University of Wisconsin-Madison, 1998.

15 Asiri A M, Akkurt M, Khan S A, Khan I U & Arshad M N, *Acta Cryst*, 65 (2009) 1303.

16 Varsanyi G, *Assignments for vibrational spectra of seven hundred benzene derivatives*, (Adam Hilger: London), 1974.

17 Karabacak M, Postalcilar E & Cinar M, *Spectrochim Acta A*, 85 (2012) 261.

18 Lin V D, Clothip N B, Fatelly W G & Granelli J G, *The hand book about infrared and Raman characteristics frequencies of organic molecules*, (Academic press: Boston), 1991.

19 Sajan D, Binoy J, Pradeep B, Krishnan K V, Kartha V B, Joe I H & Jayakumar V S, *Spectrochim Acta A*, 60 (2004) 173.

20 Ristova M, Pejov L, Zugic M & Soptrajanov B, J Mol Struct, 482 (1999) 647.

21 Hasegawa K, Ono T & Noguchi T, *J Phys Chem B*, 104 (2004) 4253.

22 Silverstein M, Basseler G C & Morill C, *Spectrometric identification of organic compounds*, (Wiley: New York), 1981.

23 Krishnakumar V & Balachandran V, *Spectrochim Acta*, 61 (2005) 1001.

24 Sathyanarayana D N, *Vibrational spectroscopy theory and applications*, (New Age International Publishers: New Delhi), 2004.

25 Subaschandrabose S, Saleem H, Erdogdu Y, Rajarajan G & Thanikachalam V, *Spectrochim Acta*, 82 (2011) 260.

26 Gnanasambandan T, Gunasekaran S & Seshadri S, *Spectrochim Acta*, 117 (2014) 557.

27 Geskin V M, Lambert C & Bredas J L, *J Am Chem Soc*, 125 (2003) 15651.

28 Sajan D, Joe H, Jayakumar V S & Zaleski J, *J Mol Struct*, 785 (2006) 43.

29 Pearson R G, *J Org Chem*, 54 (1989) 1423.

30 Lewis D F V, Loannides C & Parke D V, *Xenobiotica*, 24 (1994) 401.

31 Parr R G, Donnelly R A, Levy M & Palke W E, *J Chem Phys*, 68 (1978) 3801.

32 Al-Wabli R I, Al-Ghamdi A R, Ghabbour H A, Al-Agamy M H & Monicka J C, *Molecules*, 22 (2017) 373.

33 Foster J P & Weinhold F, *J Am Chem Soc*, 102 (1980) 7211.

34 Snehalatha M, Ravi K C, Hubert J I, Sekar N & Jayakumar V S, *Spectrochim Acta*, 72 (2009) 654.

35 Kolandaivel P, Praveen G & Selvarengan P, *J Chem Sci*, 117 (2005) 591.

36 Luque F J, Lopez J M & Orazco M, *Theor Chem Acc*, 103 (2000) 343.

37 Okulik N & Jubert A H, *Int Elect J Mol Des*, 4 (2005) 17.

38 Ozdemir N, Eren B, Dincer M & Bekdemir Y, *Mol Phys*, 108 (2010) 13.

39 Politzer P & Murray J S, *Theor Chem Acc*, 108 (2002) 134.

40 Scrocco E & Tomasi J, *Adv Quant Chem,* 11 (1979) 115.

41 Luque F J, Lopez J M & Orozco M, *Theor Chem Acc*, 103 (2000) 343.

42 Okulik N & Jubert A H, *J Mol Des*, 4 (2005) 17.

43 Murray J S & Sen K, *Molecular electrostatic potentials. Concepts and applications*, (Elsevier: Amsterdam), 1996.

44 Seminario J M, *Recent development and applications of modern density functional theory*, (Elsevier: Amsterdam), 1996.

45 Irikura K K & Thermo P L, *National Institute of Standards and Technology*, (Gaithersburg: M D), 2002.

46 Bevan O J & Boerio-Goates J, *Calculations from statistical thermodynamics*, (Academic Press), 2000.

47 Sajan D, Josepha L, Vijayan N & Karabacak M, *Spectrochim Acta*, 81A (2011) 85.

48 Zhang R, Dub B, Sun G & Sun Y, *Spectrochim Acta*, 75A (2010) 1115.